J. Fluid Mech. (2000), *vol.* 406, *pp.* 199–219. Printed in the United Kingdom

The anomalous motion of superfluid helium in a rotating cavity

By KAREN L. HENDERSON[1] AND CARLO F. BARENGHI[2]

[1]Faculty of Computer Studies and Mathematics, University of the West of England, Bristol, BS16 1QY, UK
e-mail: Karen.Henderson@uwe.ac.uk

[2]Department of Mathematics, University of Newcastle, Newcastle upon Tyne, NE1 7RU, UK
e-mail: C.F.Barenghi@ncl.ac.uk

(Received 13 August 1998 and in revised form 21 August 1999)

We numerically solve the nonlinear two-fluid Hall–Vinen–Bekharevich–Khalatnikov (HVBK) equations for superfluid helium confined inside a short Couette annulus. The outer cylinder and the ends of the annulus are held fixed whilst the inner cylinder is rotated. This simple flow configuration allows us to study how the vortex lines respond to a shear in the presence of boundaries. It also allows us to investigate further the boundary conditions associated with the HVBK model. The main result of our investigation is the anomalous motion of helium II when compared to a classical fluid. The superfluid Ekman cells always rotate in the opposite sense to a classical Navier–Stokes fluid due to the mutual friction between the two fluids, whilst the sense of rotation of the normal fluid Ekman cells depends on the parameter range considered. We also find that the tension of the vortex lines forces the superfluid to rotate about the inner cylinder almost like a rigid column.

1. Introduction and motivation

When the temperature T of liquid helium is reduced below the lambda point, $T = T_\lambda = 2.172\,\mathrm{K}$, a phase transition takes place and liquid helium becomes a quantum fluid called *helium II*. Helium II has very unusual properties, the study of which is a major topic of condensed matter physics. Our concern is the *macroscopic* dynamics of helium II. By macroscopic we mean that we are interested in phenomena which take place on a scale much larger than the interatomic spacing traditionally of interest to the condensed matter physicists. In particular we want to investigate the nature of the flow of helium II and how it differs from the flow of a classical fluid such as water: this is the realm of superfluid hydrodynamics. There are two more motivations to study the hydrodynamics of a superfluid. The first arises from the engineering applications: helium is the only substance available in liquid form at temperatures near absolute zero, so it is important as a cryogenics coolant. Applications range from infrared detectors in Space science to the cooling of superconducting magnets in particle physics. The second motivation comes from recent experimental developments in which the relation between classical and quantum turbulence is investigated (Donnelly 1991*a*; Smith *et al.* 1993 ; Barenghi, Swanson & Donnelly 1995; Barenghi *et al.* 1997; Nore, Abid & Brachet 1997*a*, *b*; Maurer & Tabeling 1998; Melotte & Barenghi 1998), including the construction of a superfluid wind tunnel.

The fluid dynamics picture of helium II dates back to Landau's *two-fluid model* (Landau & Lifshitz 1987), in which helium II is described as the intimate mixture of two fluid components, the inviscid *superfluid* and the viscous *normal fluid*. The former corresponds to the quantum mechanical ground state and is similar to a classical inviscid Euler fluid. The latter arises from the thermal excitations (similar to the phonons of solid state physics) and is similar to a classical viscous Navier–Stokes fluid. The relative proportion of superfluid and normal fluid is determined by the temperature: at $T = 0$ helium II is entirely superfluid, while at $T \geqslant T_\lambda$ it is entirely 'normal' and behaves like an ordinary classical fluid called helium I. Provided that the sample of helium II under investigation does not contain vortex lines, Landau's theory gives a detailed account of all observed phenomena, including some famous effects which seemed paradoxical to the early investigators, for example the frictionless motion in thin capillaries, the fountain effect, the existence of second sound and superleaks.

It is the vortex lines which make the hydrodynamics of helium II particularly interesting (Donnelly 1991*b*). They appear in the superfluid component when helium II rotates or when it moves along a tube faster than a small critical velocity. They also introduce dissipation and limit the otherwise perfect heat conducting property of the superfluid, which affects the engineering applications. A vortex line in helium II consists of a very small hollow core region (of radius $a_0 \approx 10^{-8}$ cm) around which the superfluid velocity field $\boldsymbol{v}^s$ spins with fixed circulation, given by the relation

$$\int_{\mathscr{C}} \boldsymbol{v}^s \cdot \mathrm{d}\boldsymbol{l} = \Gamma, \tag{1.1}$$

where $\mathscr{C}$ is a path around the vortex core and the quantum of circulation $\Gamma = 0.97 \times 10^{-3}\ \mathrm{cm^2\ s^{-1}}$ is the ratio of Plank's constant and the mass of an atom of helium.

Because of the smallness of Γ the typical flow of helium II contains a very large number of vortex lines. For example, if helium II is contained inside a cylinder and rotates as a solid body at constant angular velocity Ω, vortex lines appear in the superfluid; they are aligned along the axis of rotation and form a uniform array with areal density $2\Omega/\Gamma$ (Feynman 1955), which is approximately 10^4 lines per square centimetre at the frequency of rotation of 1 Hz. Now there are two lines of attack to the problem of understanding the flow of helium II in the presence of vortices. The first approach was pioneered by Schwarz (1982, 1985, 1988); it consists of performing direct numerical simulations in which the motion of individual vortex lines is integrated in time in the presence of a given normal fluid using the laws of vortex dynamics (the Biot-Savart rule or its local induction approximation). This approach, which was followed up by other investigators (Samuels 1992; Aarts & deWaele 1994), has shed light onto the problem of quantum turbulence (Nemirowskii & Fiszdon 1995; Tough 1982). Unfortunately it has two drawbacks: since the individual motion of many vortex lines must be determined, it is computationally very expensive, and it is not dynamically self-consistent because there is no feedback of the vortices onto the imposed normal fluid. The second approach is based on a continuum approximation which generalizes Landau's two-fluid theory; the approximation is justified by the large density of vortices which is typically present in the flow. The advantage is that it is less computationally expensive and it is self-consistent. It is the second approach which we investigate in this paper.

In Landau's original two-fluid theory the superfluid is irrotational, but it is possible to modify Landau's equations to take into account the existence of quantized vorticity. A new set of equations, referred to as the HVBK model in the literature, was derived

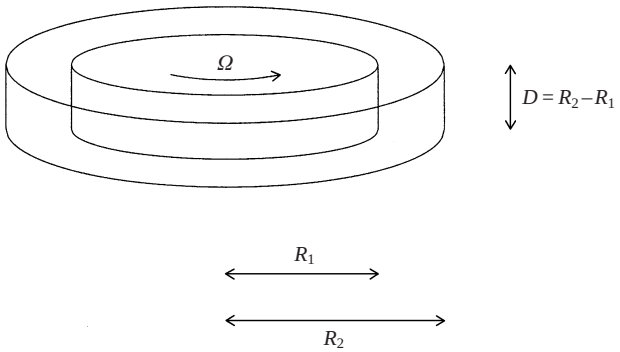

FIGURE 1. The problem's configuration. The fluid is contained inside a cylindrical box of inner radius R_1, outer radius R_2, height D and gap $R_2 - R_1 = D$. The inner cylinder rotates at constant angular velocity Ω, while the outer cylinder and the top and bottom end plates are stationary.

by a number of people over the years to describe a continuum in which a fluid particle is a small but macroscopic region which is threaded by a high density of vortex lines, all pointing almost in the same direction (Hall & Vinen 1956; Hall 1960; Khalatnikov 1965; Hills & Roberts 1977). Together with the vortex lines, the HVBK model introduces two new physical effects which are absent in Landau's theory. The first is that the superfluid vortex lines scatter the thermal excitations, thus introducing a coupling force between normal fluid and superfluid components called the mutual friction force; this effect is important in problems of heat flow because it leads to extra dissipation. The second effect is that the vortex lines have energy per unit length, that is tension. Because of the tension, the vortex lines which thread a fluid particle can oscillate (vortex waves), thus giving the superfluid an intrinsic springiness.

Actual solutions of the HVBK equations have been obtained only for a small number of flows. In particular it is worth mentioning three flows. The first is the very simple, almost trivial case of solid body rotation inside a rotating cylinder (Hall 1960), which was historically the first flow to be explored and clarified the concept of mutual friction. The second is flow in a cylindrical pipe (Geurst 1979). Theoretically, this is still a rather unexplored area which has connection with heat transfer and the study of quantum turbulence. A related problem which involves studying boundary effects and modelling turbulent helium flow was considered by Fiszdon *et al.* (1994). The third flow is Couette flow between two infinitely long, concentric, rotating cylinders. Despite the large number of experiments (see the review by Donnelly & LaMar 1988) and the early pioneering theoretical attempts of Chandrasekhar & Donnelly (1957) and Snyder (1974), it took a long time to understand the nature of helium Couette flow and make contact between theory (Barenghi & Jones 1987; Barenghi 1992) and experiments (Swanson & Donnelly 1991; Bielert & Stamm 1993). Recent theoretical work on Couette flow includes the study of nonlinear Taylor flow (Henderson, Barenghi & Jones 1995; Henderson & Barenghi 1994) and provides the best test of the validity of the HVBK model.

The aim of this paper is to study another simple laminar flow in order to gain more insight into the hydrodynamics of helium II. The problem which we have chosen is the flow of a fluid which is confined radially between two concentric cylinders of inner and outer radius R_1 and R_2, and axially between two fixed plates which are separated by the distance $D = R_2 - R_1$, see figure 1. The top and bottom plates and the outer cylinder are held stationary and the inner cylinder rotates at constant angular

velocity Ω, thus introducing shear into the system. Essentially, what we study is unit-aspect-ratio Couette flow. This flow has two key features: the shear and the fact it is dominated by end effects in all directions, both parallel and perpendicular to the natural axial direction of the vortex lines in a rotating system. How these two features affect the quantized vorticity is a problem which has never been tackled before. The first feature (the shear) makes our flow different from the solid-body rotating cylinder mentioned earlier, while the second feature (the end plates) makes it different from Couette flow between infinitely long cylinders which we have already studied. The second feature also allows us to study the issue of the boundary conditions, which is a delicate topic of the HVBK theory (Henderson *et al.* 1995).

Understanding this flow is also a necessary step in view of future work in which we plan to study the transition from Couette flow to Taylor vortices at finite values of aspect ratio $h = H/D$ where H is the height of the cylinders. Previous work on the transition was carried out in the infinite cylinder approximation $h \to \infty$. Unfortunately this approximation fails at low temperatures, because the critical axial wavenumber of the instability, calculated from linear stability analysis, tends to zero as $T \to 0$ (Barenghi & Jones 1987). This effect is so pronounced that, in a typical apparatus, even at a temperature as high as $T = 2\,\mathrm{K}$ the Taylor vortex cells are so elongated in the axial direction that the flow is dominated by what happens at the ends. So the study of end effects is related to the study of flows of helium II at temperatures closer to absolute zero. The importance of end effects was not apparent to the early experimentalists who studied helium Couette flow. Unlike water, helium II cannot be easily visualized, and they were misled by the analogy with classical Couette flow in which the Taylor cells have size of the order of the gap's width D for which if H/D is sufficiently large end effects do not matter. There is only one experiment in which a successful flow visualization was carried out in helium II using glass microspheres, but it involved turbulent flows (Bielert & Stamm 1993). So one of our aims is to provide some 'theoretical flow visualization' and highlight similarities and differences between the flow patterns of helium II and those of a classical Navier–Stokes fluid.

The plan of the paper is as follows: Section 2 provides the necessary background to superfluid hydrodynamics. Section 3 introduces the governing equations. The boundary conditions and the method of solution are discussed in § 4 and § 5. Section 6 describes the results. Finally § 7 draws some conclusions.

2. The two-fluid theory

We consider helium II at the constant temperature T and call $\boldsymbol{v}^n$ and $\boldsymbol{v}^s$ the normal fluid and superfluid velocity fields, ρ^n and ρ^s the normal fluid and superfluid densities, $\rho = \rho^n + \rho^s$ helium's total density, p^n and p^s effective pressures and ν^n the normal fluid kinematic viscosity. The relative amount of normal fluid and superfluid present in the flow depends on the temperature of the liquid: if $T \to T_\lambda$ then $\rho^s/\rho \to 0$ and $\rho^n/\rho \to 1$; if $T \to 0$ then $\rho^s/\rho \to 1$ and $\rho^n/\rho \to 0$. The incompressible isothermal HVBK equations of motion of the two fluids are

$$\frac{\partial \boldsymbol{v}^n}{\partial t} + (\boldsymbol{v}^n \cdot \nabla)\boldsymbol{v}^n = -\nabla p^n + \nu^n \nabla^2 \boldsymbol{v}^n + \frac{\rho^s}{\rho}\boldsymbol{F}, \tag{2.1}$$

$$\frac{\partial \boldsymbol{v}^s}{\partial t} + (\boldsymbol{v}^s \cdot \nabla)\boldsymbol{v}^s = -\nabla p^s - \nu^s \boldsymbol{T} - \frac{\rho^n}{\rho}\boldsymbol{F}, \tag{2.2}$$

$$\nabla \cdot \boldsymbol{v}^n = 0, \qquad \nabla \cdot \boldsymbol{v}^s = 0. \tag{2.3}$$

What makes the HVBK equations different from Landau's two-fluid equations is the existence of a *macroscopic* vorticity field

$$\boldsymbol{\omega}^s = \nabla \times \boldsymbol{v}^s, \tag{2.4}$$

and the introduction of the mutual friction force $\boldsymbol{F}$ and the vortex tension force $-v^s \boldsymbol{T}$. Essentially, the superfluid vorticity $\boldsymbol{\omega}^s$ is a measure of how many vortex line singularities are contained in a given small region of fluid and point along a particular direction. *Microscopically* – that is to say on scales smaller than the scale described by the HVBK theory – each vortex line is a tiny hollow around which the microscopic superfluid velocity field is irrotational because it is proportional to the gradient of the phase of the quantum mechanical wave function. The HVBK equations thus represent a coarse-graining of the theory of Landau. From $\boldsymbol{\omega}^s$ we define the unit vector $\widehat{\boldsymbol{\omega}}^s$ along the vorticity field

$$\widehat{\boldsymbol{\omega}}^s = \frac{\boldsymbol{\omega}^s}{\omega^s}, \tag{2.5}$$

where $\omega^s = |\boldsymbol{\omega}^s|$. The mutual friction force is

$$\boldsymbol{F} = \tfrac{1}{2}B\widehat{\boldsymbol{\omega}}^s \times (\boldsymbol{\omega}^s \times (\boldsymbol{v}^n - \boldsymbol{v}^s - v^s \nabla \times \widehat{\boldsymbol{\omega}}^s)) + \tfrac{1}{2}B'\boldsymbol{\omega}^s \times (\boldsymbol{v}^n - \boldsymbol{v}^s - v^s \nabla \times \widehat{\boldsymbol{\omega}}^s), \tag{2.6}$$

where B and B' are coefficients which describe the interaction between the normal fluid and the vortices (Barenghi, Donnelly & Vinen 1983; Samuels & Donnelly 1990). In the regime in which the HVBK equations apply these coefficients depend only on temperature and are well known from measurements, neglecting a very weak dependence of these coefficients on the velocity and frequency (Swanson *et al.* 1987). The parameter B is always positive, whilst parameter B' is negative for temperatures above 2.06 K and positive for temperatures below 2.06 K. Finally the vortex tension force $-v^s \boldsymbol{T}$ is given by

$$\boldsymbol{T} = \boldsymbol{\omega}^s \times (\nabla \times \widehat{\boldsymbol{\omega}}^s), \tag{2.7}$$

where $v^s = (\Gamma/4\pi)\log(b_0/a_0)$ is the vortex tension parameter, a_0 is the vortex core radius and $b_0 = (\omega^s/\Gamma)^{-1/2}$ is the intervortex spacing. Note that v^s has the same dimension as a kinematic viscosity, but physically it is very different: it represents the ability of a superfluid particle to oscillate because of the vortex waves which can be excited on the vortex lines threading the particle itself.

The HVBK equations have three interesting limits. Firstly, if $T \to T_\lambda$, then $\rho^s/\rho \to 0$, $\rho^n/\rho \to 1$, helium II becomes entirely 'normal' and the the normal fluid equation (2.1) reduces to the classical viscous Navier–Stokes equation

$$\frac{\partial \boldsymbol{v}^n}{\partial t} + (\boldsymbol{v}^n \cdot \nabla)\boldsymbol{v}^n = -\nabla p^n + \nu^n \nabla^2 \boldsymbol{v}^n. \tag{2.8}$$

Secondly, if $T \to 0$, then $\rho^s/\rho \to 1$, $\rho^n/\rho \to 0$ and helium II becomes entirely 'super': the superfluid equation (2.2) reduces to the equation of a pure superflow

$$\frac{\partial \boldsymbol{v}^s}{\partial t} + (\boldsymbol{v}^s \cdot \nabla)\boldsymbol{v}^s = -\nabla p^s - v^s \boldsymbol{\omega}^s \times (\nabla \times \widehat{\boldsymbol{\omega}}^s). \tag{2.9}$$

Finally, if we set Plank's constant equal to zero, the quantum of circulation Γ vanishes, and so does v^s in which case (2.9) reduces to the classical inviscid Euler equation

$$\frac{\partial \boldsymbol{v}^s}{\partial t} + (\boldsymbol{v}^s \cdot \nabla)\boldsymbol{v}^s = -\nabla p^s. \tag{2.10}$$

It must be stressed that the HVBK model applies to helium II only if quantized

vorticity exists in the superfluid, that is to say if the angular velocity Ω exceeds the critical value

$$\Omega_C = \frac{2\Gamma}{\pi R_2 D}\left[\ln\left(\frac{2D}{\pi a_o}\right) + \frac{1}{4}\right] \tag{2.11}$$

(Swanson & Donnelly 1987). The study of flows for which Ω is approximately equal to Ω_C, that is to say of laminar flows with few superfluid vortex lines, is beyond the validity of the HVBK model (which is based on partial differential equations) and would require the approach of Schwarz (in which the motion of individual vortices is computed). Studying what happens to isolated vortex lines is important to understand the fundamental nature of friction (Barenghi *et al.* 1983; Sonin 1987; Thouless, Ao & Niu 1996), and it involves non-trivial experimental problems of detection. However, since the friction is essentially proportional to the amount of quantized vorticity, the back reaction of the vortex lines onto the normal fluid would be very small, so we would not expect the normal fluid motion to be very different from the motion of a classical Navier–Stokes fluid in this case, unlike the findings which we shall present in § 6.

Hereafter we shall thus consider situations which refer to $\Omega > \Omega_C$. Using the parameters chosen in § 6, the critical angular velocity corresponds typically to the Reynolds number $Re \approx 50$, where Re will be defined in § 3.

3. The governing equations

It is convenient to represent the velocity fields of our problem in terms of departures from azimuthal Couette flow $\boldsymbol{v}^0$. Using cylindrical coordinates (r, ϕ, z) we write

$$\boldsymbol{v}^n = \boldsymbol{v}^0 + \boldsymbol{u}^n, \qquad \boldsymbol{v}^s = \boldsymbol{v}^0 + \boldsymbol{u}^s, \tag{3.1a,b}$$

where Couette flow is

$$\boldsymbol{v}^0 = v^0_\phi \hat{\boldsymbol{\phi}} = (ar + b/r)\hat{\boldsymbol{\phi}}, \tag{3.2}$$

and $\hat{\boldsymbol{\phi}}$ is the unit vector in the azimuthal ϕ-direction. The Couette parameters a and b are defined as

$$a = -\frac{\Omega R_1^2}{(R_2^2 - R_1^2)}, \qquad b = \frac{\Omega R_1^2 R_2^2}{(R_2^2 - R_1^2)} \tag{3.3a,b}$$

(Chandrasekhar 1961) so that $v^0_\phi = \Omega R_1$ at $r = R_1$ and $v^0_\phi = 0$ at $r = R_2$. We make the simplifying assumption that the flow is axisymmetric and express $\boldsymbol{u}^n$ and $\boldsymbol{u}^s$ in terms of stream functions ψ^n and ψ^s:

$$\boldsymbol{u}^n = (u^n_r, u^n_\phi, u^n_z) = \left(-\frac{1}{r}\frac{\partial \psi^n}{\partial z}, u^n_\phi, \frac{1}{r}\frac{\partial \psi^n}{\partial r}\right), \tag{3.4}$$

$$\boldsymbol{u}^s = (u^s_r, u^s_\phi, u^s_z) = \left(-\frac{1}{r}\frac{\partial \psi^s}{\partial z}, u^s_\phi, \frac{1}{r}\frac{\partial \psi^s}{\partial r}\right). \tag{3.5}$$

Equations (3.4) and (3.5) guarantee that conditions (2.3) are automatically satisfied.

The equations are then made dimensionless using D as the unit of length and the normal fluid viscous time scale D^2/ν^n as the unit of time. This choice allows us to recover smoothly the classical limit $T \to T_\lambda$ and study the case of a classical viscous Navier–Stokes flow for comparison. The model's equations are obtained by considering the ϕ-components of (2.1) and (2.2) and the ϕ-components of the curl of

(2.1) and (2.2):

$$\frac{\partial u_\phi^n}{\partial t} = \mathrm{L}_1 u_\phi^n + N_1, \qquad \frac{\partial \omega_\phi^n}{\partial t} = \mathrm{L}_1 \omega_\phi^n + N_2, \tag{3.6}$$

$$\frac{\partial u_\phi^s}{\partial t} = N_3, \qquad \frac{\partial \omega_\phi^s}{\partial t} = N_4. \tag{3.7a,b}$$

These equations must be solved in $r_1 \leqslant r \leqslant r_2$, $0 \leqslant z \leqslant 1$, where $r_1 = R_1/D$ and $r_2 = R_2/D$, together with the conditions which link the stream functions ψ^n and ψ^s to the azimuthal components of the vorticities

$$\mathrm{L}_2 \psi^n = -r\omega_\phi^n, \qquad \mathrm{L}_2 \psi^s = -r\omega_\phi^s. \tag{3.8a,b}$$

L_1 and L_2 are linear operators defined by

$$\mathrm{L}_1 = \frac{\partial^2}{\partial x^2} + \frac{1}{r}\frac{\partial}{\partial x} - \frac{1}{r^2} + \frac{\partial^2}{\partial z^2}, \tag{3.9}$$

$$\mathrm{L}_2 = \frac{\partial^2}{\partial x^2} - \frac{1}{r}\frac{\partial}{\partial x} + \frac{\partial^2}{\partial z^2}, \tag{3.10}$$

where $x = r - r_1$, and N_1, N_2, N_3 and N_4 are the nonlinear quantities

$$N_1 = \frac{1}{r}\left(2a + \frac{u_\phi^n}{r}\right)\frac{\partial \psi^n}{\partial z} + \frac{1}{r}\frac{\partial(\psi^n, u_\phi^n)}{\partial(z,x)} + \frac{\rho^s}{\rho}F_\phi, \tag{3.11}$$

$$N_2 = \frac{2}{r}(u_\phi^0 + u_\phi^n)\frac{\partial u_\phi^n}{\partial z} - \frac{\omega_\phi^n}{r^2}\frac{\partial \psi^n}{\partial z} + \frac{1}{r}\frac{\partial(u_\phi^n, \psi^n)}{\partial(x,z)} + \frac{\rho^s}{\rho}\left(\frac{\partial F_r}{\partial z} - \frac{\partial F_z}{\partial x}\right), \tag{3.12}$$

$$N_3 = \frac{1}{r}\left(2a + \frac{u_\phi^s}{r}\right)\frac{\partial \psi^s}{\partial z} + \frac{1}{r}\frac{\partial(\psi^s, u_\phi^s)}{\partial(z,x)} - \frac{\rho^n}{\rho}F_\phi - \beta T_\phi, \tag{3.13}$$

$$N_4 = \frac{2}{r}(u_\phi^0 + u_\phi^s)\frac{\partial u_\phi^s}{\partial z} - \frac{\omega_\phi^s}{r^2}\frac{\partial \psi^s}{\partial z} + \frac{1}{r}\frac{\partial(u_\phi^s, \psi^s)}{\partial(x,z)} - \frac{\rho^n}{\rho}\left(\frac{\partial F_r}{\partial z} - \frac{\partial F_z}{\partial x}\right) - \beta\left(\frac{\partial T_r}{\partial z} - \frac{\partial T_z}{\partial x}\right), \tag{3.14}$$

where

$$\frac{\partial(f,g)}{\partial(x,y)} = \frac{\partial f}{\partial x}\frac{\partial g}{\partial y} - \frac{\partial f}{\partial y}\frac{\partial g}{\partial x}$$

and $-\beta \boldsymbol{T} = -\beta(T_r, T_\phi, T_z)$ is the dimensionless vortex tension force and $\boldsymbol{F}$ is now the dimensionless mutual friction.

The solution of the dimensionless nonlinear equations (3.6)–(3.8) is obtained by direct time integration starting from an arbitrary configuration. The actual computational box is $0 \leqslant z \leqslant 1$ and $0 \leqslant x \leqslant 1$. The input parameters are the radius ratio $\eta = R_1/R_2$, the Reynolds number $Re = \Omega R_1 D/\nu^n$, which is the dimensionless velocity of the inner cylinder, and helium's temperature T. The temperature determines the normal fluid and superfluid ratios ρ^s/ρ and ρ^n/ρ, the mutual friction coefficients B and B' and the dimensionless vortex tension parameter $\beta = \nu^s/\nu^n$.

Note that we need the actual size D of the system to determine ν^s, which is proportional to the logarithm of the ratio of the average distance between vortex lines b_0 and the vortex core radius a_0. This extra dimensional input would not be necessary if we had chosen the vortex core a_0 as the unit of length, which is of course too small. What we do in practice is to use the size $D = 0.0474\,\mathrm{cm}$ of Swanson & Donnelly's helium apparatus at the University of Oregon. The results do not depend

much on this choice because it is only the logarithm of b_0/a_0 which is used. In the same spirit we approximate $b_0 = (\omega^s/\Gamma)^{-1/2} \approx (2|a|/\Gamma)^{-1/2}$.

4. The boundary conditions

The system of equations (3.6)–(3.8) requires three boundary conditions for the normal fluid and three boundary conditions for the superfluid at each boundary. These boundary conditions are not determined by the HVBK model itself, but are extra requirements which we impose to model the physics of the fluid–boundary interaction.

The normal fluid is viscous, hence it must satisfy standard no-slip boundary conditions. These conditions are that $\boldsymbol{v}^n = 0$ at all stationary boundaries $z = 0$, $z = 1$ and $r = r_2$, and that $\boldsymbol{v}^n = Re\hat{\boldsymbol{\phi}}$ at the moving boundary $r = r_1$. Taking (3.1a) into account we have

$$u^n_\phi(r_1, z) = u^n_\phi(r_2, z) = 0, \tag{4.1}$$

$$u^n_\phi(r, 0) = u^n_\phi(r, 1) = -v^0_\phi, \tag{4.2}$$

$$\psi^n(r_1, z) = \psi^n(r_2, z) = \psi^n(r, 0) = \psi^n(r, 1) = 0, \tag{4.3}$$

$$\frac{\partial \psi^n}{\partial r}(r_1, z) = \frac{\partial \psi^n}{\partial r}(r_2, z) = \frac{\partial \psi^n}{\partial z}(r, 0) = \frac{\partial \psi^n}{\partial z}(r, 1) = 0. \tag{4.4}$$

The superfluid's boundary conditions are more delicate. The superfluid is inviscid. In the absence of vortex lines it need only satisfy the condition that there is no flow across all boundaries, without any restriction on the tangential motion: slip is allowed. This requirement, that $v^s_r = 0$ at $r = r_1$ and $r = r_2$ and that $v^s_z = 0$ at $z = 0$ and $z = 1$, is equivalent to

$$\psi^s(r_1, z) = \psi^s(r_2, z) = 0, \tag{4.5}$$

$$\psi^s(r, 0) = \psi^s(r, 1) = 0. \tag{4.6}$$

Extra conditions are introduced by the presence of the vortex lines. In our previous paper (Henderson *et al.* 1995) we studied Couette flow between infinitely long cylinders and argued that the conditions at the boundaries $r = r_1$ and $r = r_2$ parallel to the rotation-induced superfluid vorticity are

$$\omega^s_\phi(r_1, z) = \omega^s_\phi(r_2, z) = 0, \tag{4.7}$$

$$u^s_\phi(r_1, z) = u^s_\phi(r_2, z) = 0. \tag{4.8}$$

Equation (4.7) implies that the azimuthal velocity of the superfluid at $r = r_1$ and $r = r_2$ is the same as that of the cylinders; thus the superfluid slips only in the axial direction, at the cylinder walls. Equation (4.8) also implies that $\omega^s_r = 0$ at $r = r_1$ and r_2. Because of (4.7), this means that the only superfluid vorticity which exists at the walls is aligned along the z-direction, which is the axis of rotation. This is the natural orientation of the vortex lines in the case a solid-body rotating cylinder or annulus, and also in the case of Couette flow, provided that Ω is smaller than the critical value for the onset of Taylor vortex flow. The fact that both the superfluid velocity and the superfluid vorticity are parallel near the cylindrical walls means that there is no mutual friction there. Calculations of nonlinear Taylor flow performed using (4.7) and (4.8) gave results which are in agreement with torque and second sound measurements (Henderson & Barenghi 1994; Henderson *et al.* 1995). The drawback of using (4.7)

and (4.8) is that one neglects a small vortex-free region near the walls. The vortex-free region was also neglected in the linear stability calculations (Barenghi 1992) which predicted with success the observed appearance of Taylor vortex flow. There are theoretical reasons for the existence of the vortex-free region, and its existence has been observed in some experiments involving a rotating annulus. However it is not clear how to describe it in the context of a continuum model (the HVBK theory) based on a high density of vortex filaments. Fortunately it is apparent from the agreement with the measurements obtained using (4.7) and (4.8) that the vortex-free region must have only a limited effect on the main flow, and hereafter we neglect it and adopt conditions (4.7) and (4.8).

The situation is very different at the boundaries $z = 0$ and $z = 1$ which are perpendicular to the rotation axis, z. In the related configurations of a cylinder or an annulus, which rotate as a solid body, the vortex lines would naturally meet these boundaries in a perpendicular fashion. This leads us to assume that the vortex lines are purely axial at $z = 0$ and 1, that is to say

$$\omega_r^s(r,0) = \omega_r^s(r,1) = 0, \tag{4.9}$$

$$\omega_\phi^s(r,0) = \omega_\phi^s(r,1) = 0. \tag{4.10}$$

Equation (4.9) is equivalent to

$$\frac{\partial u_\phi^s}{\partial z}(r,0) = \frac{\partial u_\phi^s}{\partial z}(r,1) = 0. \tag{4.11}$$

The superfluid's boundary conditions have been discussed by Khalatnikov (1965) who argued that the vortex lines can either slide at the boundary or remain totally or partially pinned at some small geometrical imperfection. Khalatnikov argues that the velocity, $\boldsymbol{v}^L$ of a vortex line at a stationary boundary has tangential components given by

$$\boldsymbol{v}^L = c_1 \hat{\boldsymbol{n}} \times (\hat{\boldsymbol{n}} \times \widehat{\boldsymbol{\omega}}^s) - c_2 \hat{\boldsymbol{n}} \times \widehat{\boldsymbol{\omega}}^s, \tag{4.12}$$

where $\hat{\boldsymbol{n}}$ is the unit vector normal to the surface and c_1 and c_2 are coefficients which describe the interaction of the vortices with the boundary. Total pinning of the vortices to the end plates at $z = 0$ and $z = 1$ cannot occur, because each rotation would wrap up the vortex lines until de-pinning takes place. So what is likely to take place is partial or perfect sliding, depending on the nature and the smoothness of the boundaries. The most interesting case, which avoids introducing unknown parameters, is the case of perfect sliding, which corresponds to $c_1 \to \infty$ and $c_2 \to \infty$ in Khalatnikov's theory. This requires that $\hat{\boldsymbol{n}} \times \widehat{\boldsymbol{\omega}}^s = 0$, which is equivalent to our boundary conditions $\omega_r^s = \omega_\phi^s = 0$. In conclusion, the conditions (4.10) and (4.11) which we adopt refer to Khalatnikov's perfect sliding.

5. Numerical method

Equations (3.6) and (3.7) are time stepped forward in time starting from an arbitrary initial condition, which is either a very small seed field or a steady solution previously obtained at some other values of the input parameters. The equations are discretized on a mesh of radial points x_i ($i = 0, 1, 2, \ldots N$) and axial points z_j ($j = 0, 1, 2, \ldots M$). The spatial discretization is based on a fourth-order method at all points including the boundary points. The time stepping from time t_k to time $t_{k+1} = t_k + \Delta t$, where Δt is a small time step, is based on the ADI method for the diffusion operators L_1 appearing in (3.6). Each time step is divided into two Euler half-steps, the first implicit

in x and explicit in z, the second explicit in x and implicit in z. All other terms of the equations are time stepped using Adams–Bashforth's explicit method. When u_ϕ^n, ω_ϕ^n, u_ϕ^s and ω_ϕ^s are found at $t = t_{k+1}$ the Poisson's equations (3.8) are solved to determine ψ^n and ψ^s at the new time. This is done simply by direct inversion of the operator L_2 which appears in (3.8); the matrix which corresponds to the inverse operator is pre-calculated using a NAG routine before performing the actual time stepping.

Note that the boundary conditions (4.1) and (4.2) are used when solving the equation for u_ϕ^n, while the conditions (4.3) are used to solve the Poisson's equation for ψ^n. The boundary conditions on ω_ϕ^n are obtained using the boundary conditions on ψ^n (4.3), (4.4) and the equation relating ψ^n and ω_ϕ^n (3.8*a*). Equation (3.8*a*) is evaluated at the point $x = 0$ to give

$$-r_0\omega_{0,j}^n = \left(\frac{\partial^2\psi^n}{\partial x^2}\right)_{0,j} \tag{5.1}$$

where $\omega_{i,j}^n = \omega_\phi^n(x_i, z_j)$ and $r_0 = \eta/(1-\eta)$. Using the fourth-order forward difference formula for $(\partial^2\psi^n/\partial x^2)_{0,j}$ given that $\psi_{0,j}^n = (\partial\psi^n/\partial x)_{0,j} = 0$ we thus find that

$$\omega_{0,j}^n = -\frac{576\psi_{1,j}^n - 216\psi_{2,j}^n + 64\psi_{3,j}^n - 9\psi_{4,j}^n}{72r_0(\Delta x)^2}. \tag{5.2}$$

Boundary conditions at $x = 1$, $z = 0$ and $z = 1$ are obtained in the same way.

For the superfluid we use (4.7) and (4.10) when solving the equation for ω_ϕ^s, (4.8) and (4.11) when determining u_ϕ^s, and (4.5) and (4.6) when solving the Poisson's equation for ψ^s. Note that unlike all other equations which are solved on the internal points only, u_ϕ^s must be determined on the boundaries x_0, x_N, z_0 and z_M too; this is achieved by using fourth-order forward/backward difference formulae to calculate the derivatives.

We use a uniform x_i, z_j mesh, unlike Cliffe (1983) for example who studied very small-aspect-ratio classical Couette flow and introduced mesh refinement in the corner. No mesh refinement was used in similar studies of classical Couette flow such as Lucke, Mihelicic & Wingerath (1984) or Pfister *et al.* (1988). After a preliminary investigation, in order to improve the numerical resolution near the end plates, we decided to restrict our study to solutions which are symmetric around the midplane $z = \frac{1}{2}$. This is done by requiring that ψ^n and ψ^s are antisymmetric around the midplane and by determining them only in the half-space $k = 0, \ldots M/2$, with $\psi^n = \psi^s = 0$ at $z = \frac{1}{2}$. In this way the size of the matrix used to invert the Poisson's equations is reduced and more mesh points are used to resolve what happens near a single end plate. For the sake of clarity the results plotted in § 6 illustrate the flow in the entire cavity. Before restricting the symmetry in this way, low-resolution runs did not detect any solution in which the symmetry was broken in the range of parameters used. In the classical Couette problem at very small aspect ratio (typically $h < 1$) it is known that there are such asymmetric solutions called the anomalous modes; they consist of a single large cell which occupies almost the entire box and a very small eddy in a corner. These solutions occur however at Reynolds numbers higher than the values which we have investigated.

Finally we remark that the number of mesh points used is typically $N = 16$ and $M = 32$, which is sufficient to achieve numerical convergence. We have also tested our results using a higher number of points; the code appears robust enough to give qualitatively good solutions using rather small values of N and M around 10. This is consistent with what was reported by Pfister *et al.* (1988) who used typically only

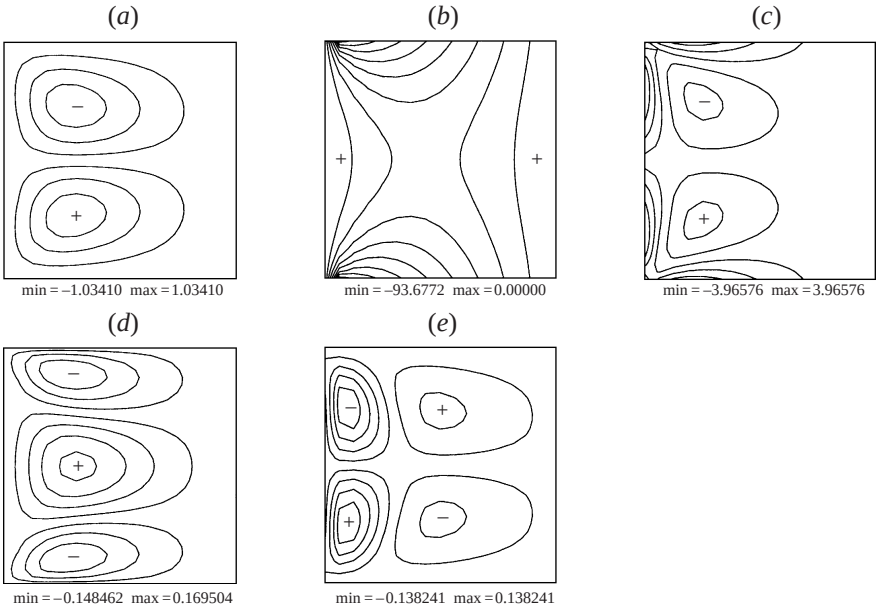

FIGURE 2. Motion of a classical fluid at $\eta = 0.976$ and $Re = 100$: (*a*) stream function ψ; (*b*) azimuthal velocity u_ϕ; (*c*) azimuthal vorticity ω_ϕ; (*d*) radial velocity u_r; (*e*) axial velocity u_z.

$N = 20$ and $M = 10$. The size of the time step which we have used is typically $\Delta t = 10^{-4}$, and the equations are integrated for a number of steps equivalent to a few dimensionless units of time, until the solution has settled down and has become time-independent.

6. Results and their interpretation

The results of the calculation of the nonlinear HVBK equations are given in figures 2–8, 10 and 11 which show contour plots of various quantities. Each figure extends over the whole computational domain $0 \leqslant x \leqslant 1$, $0 \leqslant z \leqslant 1$ with the inner cylinder and outer cylinder on the left and right respectively. Before considering helium II, it is instructive to make clear the motion of a classical fluid in the same configuration; this will allow us to draw comparisons between classical fluid dynamics and superfluid hydrodynamics. For the radius ratio we choose the value $\eta = 0.976$ of the helium apparatus used by Swanson & Donnelly (1987) at the University of Oregon. We set the mutual friction coefficients B and B' equal to zero so that the normal fluid equations (3.6) and (3.8*a*) reduce to the classical Navier–Stokes equation. Starting from an initial very small seed field, we integrate the equations in time until we obtain a steady solution at Reynolds number, $Re = 100$. The flow $\boldsymbol{u}$ which we obtain is a superposition of azimuthal motion u_ϕ around the inner cylinder and toroidal motion u_r and u_z in the vertical plane. The latter motion is in the form of a pair of cells similar to a Taylor vortex pair, but as it is caused by boundaries rather than a centrifugal instability, it is hereafter referred to an Ekman cell pair. Figure 2 shows contour plots of all the interesting fields: the stream function ψ, the azimuthal velocity u_ϕ, the azimuthal vorticity ω_ϕ, the radial velocity u_r and the axial velocity u_z. Note that the total azimuthal velocity is obtained by adding the Couette motion v_ϕ^0, which is z-independent, to u_ϕ. Figure 2(*a*) shows that the Ekman cells extend radially

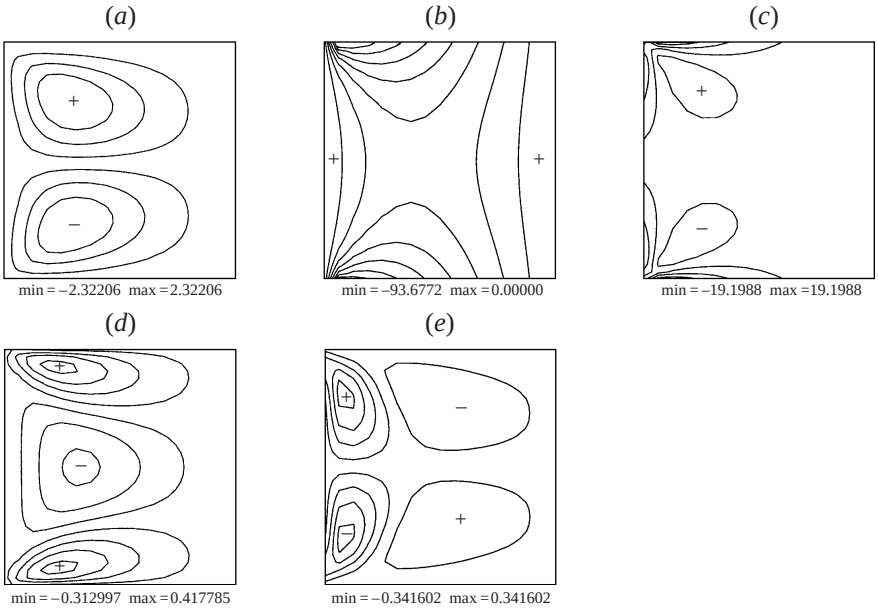

FIGURE 3. Motion of helium II in the same configuration as in figure 2 ($\eta = 0.976$ and $Re = 100$) at $T = 2.11\,\mathrm{K}$: results for the normal fluid corresponding to the results for the superfluid shown in figure 4. (*a*) Stream function ψ^n; (*b*) azimuthal velocity u^n_ϕ; (*c*) azimuthal vorticity ω^n_ϕ; (*d*) radial velocity u^n_r; (*e*) axial velocity u^n_z.

throughout the cavity. Figure 2(*b*) shows that there are horizontal layers near the stationary end plates at $z = 0$ and $z = 1$. The vorticity (figure 2*c*) has similar layers there, besides a layer at the inner cylinder $x = 0$ as well.

We now consider helium II at temperature $T = 2.11\,\mathrm{K}$. We choose this temperature as an arbitrary reference because it is high enough to make a connection to what happens in the classical limit $T \to T_\lambda = 2.172\,\mathrm{K}$, but it is also low enough that an appreciable amount of mass is superfluid ($\rho^s/\rho = 0.23$). We call the flow of helium II calculated at $T = 2.11\,\mathrm{K}$, $\eta = 0.976$ and $Re = 100$ the reference state. This flow is shown in figures 3 and 4, which refer to the normal fluid and the superfluid components respectively. The first striking result is that the normal fluid and superfluid Ekman cells rotate in the opposite direction to a classical Navier–Stokes fluid; compare figures 2(*d*), 3(*d*) and 4(*d*). In the classical case the fluid near the midplane (where the braking effect of the end plates is least) is pushed outward, so the fluid near the end plates moves inward to conserve mass. In the case of helium II both the normal fluid and the superfluid near the end plates are pushed outwards.

The other main result is the remarkable azimuthal motion u^s_ϕ of the superfluid. It is apparent from figure 4(*b*) that the superfluid rotation is almost independent of z, like the motion of a column of liquid. On the other hand the normal fluid (see figure 3*b*) and a classical fluid (see figure 2*b*) rotate in a way which is strongly affected by the ends at $z = 0$ and $z = 1$.

Now we consider the total superfluid vorticity field $\boldsymbol{\omega}^s_{\mathrm{tot}} = \boldsymbol{\omega}^s + 2a\hat{\boldsymbol{z}}$, which tells us about the superfluid vortex lines. It can be seen in figures 4(*c*), (*f*) and (*g*) that $\boldsymbol{\omega}^s_{\mathrm{tot}}$ is predominantly in the axial direction (compare the magnitudes of $\omega^s_{r,\mathrm{tot}}$, $\omega^s_{\phi,\mathrm{tot}}$ and $\omega^s_{z,\mathrm{tot}}$) and is concentrated near the inner cylinder. This theoretical prediction can be tested in an experiment by comparing the attenuation of second sound pulses sent

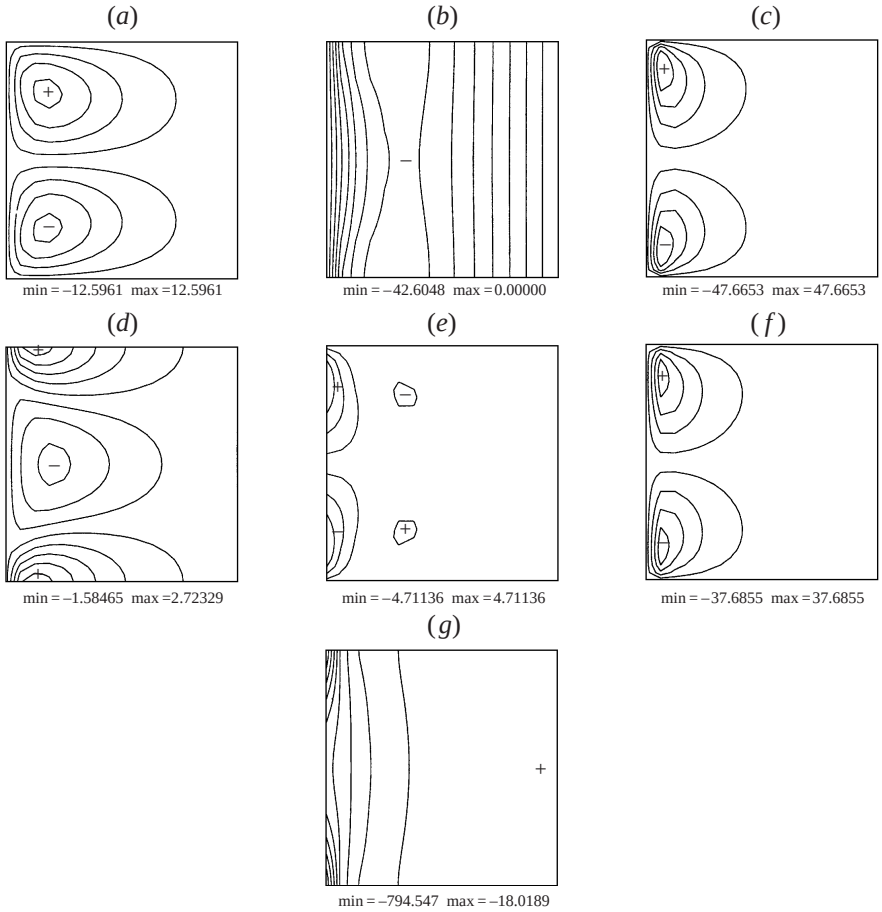

FIGURE 4. Motion of helium II in the same configuration as in figure 2 ($\eta = 0.976$ and $Re = 100$) at $T = 2.11\,\mathrm{K}$: results for the superfluid corresponding to the results for the normal fluid shown in figure 3. (*a*) Stream function ψ^s; (*b*) azimuthal velocity u^s_ϕ; (*c*) azimuthal vorticity ω^s_ϕ; (*d*) radial velocity u^s_r; (*e*) axial velocity u^s_z; (*f*) radial vorticity ω^s_r; (*g*) axial vorticity ω^s_z.

across the cell in the z-direction, using two pairs of transducers located in the inner radial region and in the outer radial region. We have seen in § 4 that with our choice of boundary conditions there is no mutual friction near the cylindrical walls. The situation is different near the end plates $z = 0$ and $z = 1$, where we expect a large mutual friction because of the different boundary conditions satisfied by the normal fluid and the superfluid.

We now study what happens if we change the temperature away from the reference level. If T is reduced below $T = 2.11\,\mathrm{K}$ the major effect is that the superfluid tends to rotate more and more like a solid column, independent of z; compare the plots of u^s_ϕ at $T = 2.11\,\mathrm{K}$ (figure 4*b*), $T = 2.08\,\mathrm{K}$ (figure 5*b*) and $T = 1.8\,\mathrm{K}$ (figure 5*a*). The normal fluid pattern does not change much, only u^n_r becomes more concentrated near the end plates. If T is increased above $T = 2.11\,\mathrm{K}$ the situation is very different. At $T = 2.15\,\mathrm{K}$ the flow pattern is similar to that showed in figures 3 and 4 but the column-like behaviour of u^s_ϕ is reduced (see figure 5*c*). A further increase in temperature to $T = 2.17\,\mathrm{K}$ makes a qualitative change: figures 6 and 7 show what happens to the normal fluid and the superfluid components. Figures 6(*a*) and 6(*d*)

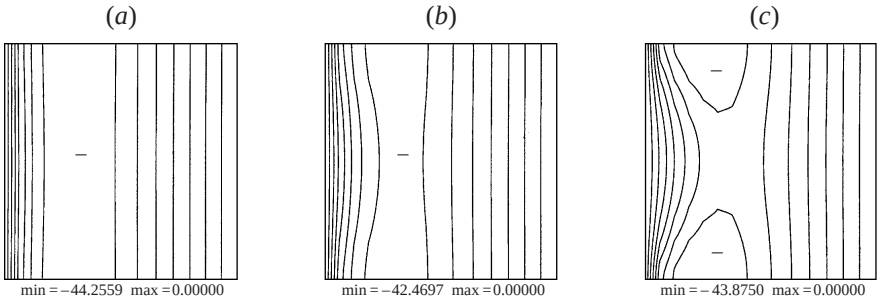

FIGURE 5. Azimuthal superfluid motion u^s_ϕ at some different temperatures. (*a*) $T = 1.8\,\mathrm{K}$; (*b*) $T = 2.08\,\mathrm{K}$; (*c*) $T = 2.15\,\mathrm{K}$. Compare with the plots at $T = 2.11\,\mathrm{K}$ in figure 4(*b*) and at $T = 2.17\,\mathrm{K}$ in figure 7(*b*). All runs at $\eta = 0.976$ and $Re = 100$.

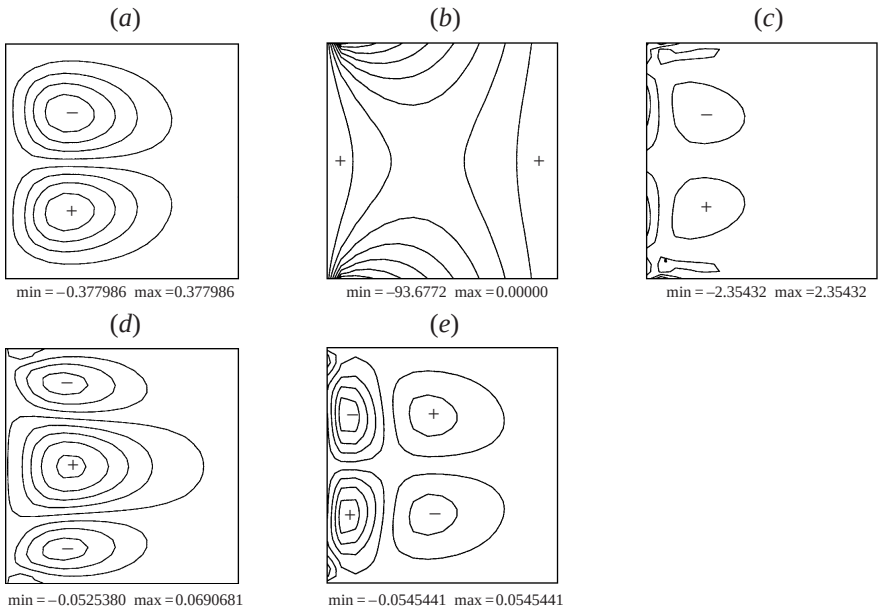

FIGURE 6. Results for the normal fluid at $T = 2.17\,\mathrm{K}$ corresponding to the results for the superfluid shown in figure 7 ($\eta = 0.976$, $h = 1$ and $Re = 100$): (*a*) stream function ψ^n; (*b*) azimuthal velocity u^n_ϕ; (*c*) azimuthal vorticity ω^n_ϕ; (*d*) radial velocity u^n_r; (*e*) axial velocity u^n_z. All runs at $\eta = 0.976$ and $Re = 100$.

show that the normal fluid Ekman cells now rotate in the same direction as the flow of a classical fluid (figures 2*a* and 2*d*), with negative radial motion near the end plates. This is what we expect for consistency, because as T approaches $T_\lambda = 2.172\,\mathrm{K}$ the superfluid fraction ρ^s/ρ vanishes and there is no mutual force to distinguish between the normal fluid of helium II and a classical fluid. The sense of rotation of the superfluid Ekman cells remains the same as it was at lower temperatures, with u^s_r positive near the end plates. The azimuthal motion of the superfluid (figure 7*b*) is now similar to that of the normal fluid, that is to say it depends strongly on z and there is no column-like pattern left. This is a consequence of the reduced dynamical importance of the superfluid: at this high temperature the density ratio is $\rho^s/\rho = 0.022$ only, so the superfluid is slaved to the normal fluid and is carried along by friction.

We shall now investigate what physical mechanism makes the superfluid rotation

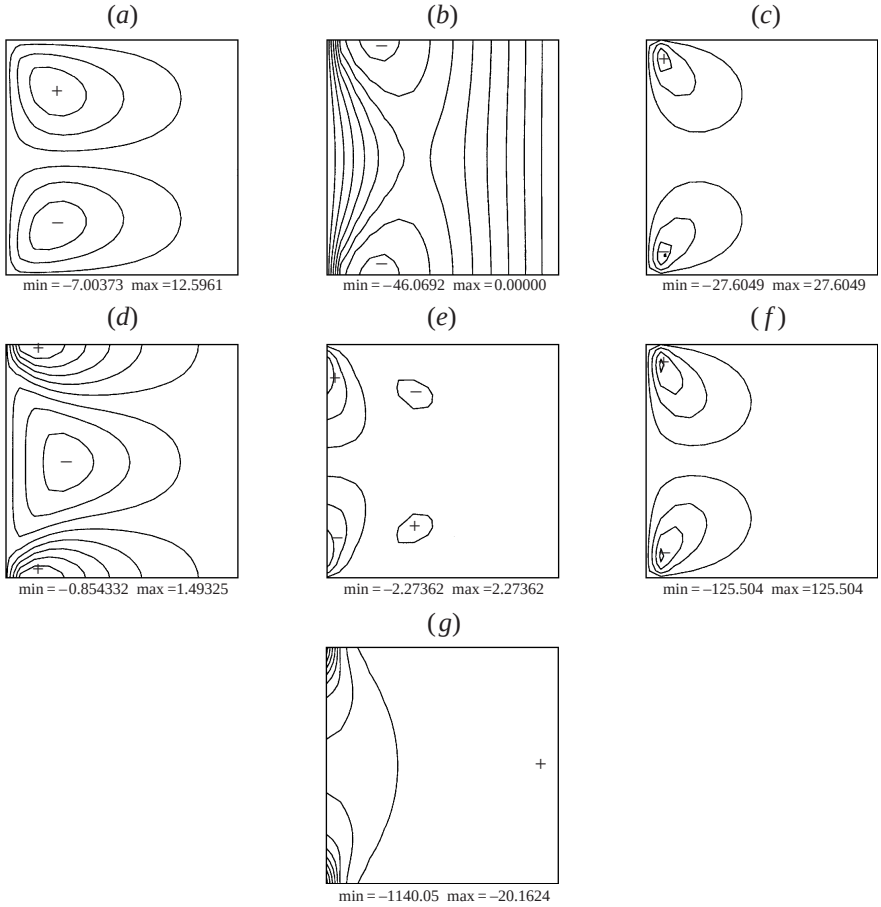

FIGURE 7. Results for the superfluid at $T = 2.17\,\mathrm{K}$ corresponding to the results for the normal fluid shown in figure 6: (*a*) stream function ψ^s; (*b*) azimuthal velocity u^s_ϕ; (*c*) azimuthal vorticity ω^s_ϕ; (*d*) radial velocity u^s_r; (*e*) axial velocity u^s_z; (*f*) radial vorticity ω^s_r; (*g*) axial vorticity ω^s_z.

u^s_ϕ to be more column-like the lower the temperature is. This tendency is not hindered by the end plates because the superfluid tangential velocity at $z = 0$ and $z = 1$ can slip, unlike what happens to u^n_ϕ which is brought to rest by the boundaries. We have performed a numerical experiment which suggests that it is the tension of the vortex lines which causes the superfluid to move in this fashion. We consider again the reference state at $T = 2.11\,\mathrm{K}$ (see figure 4*b*) and artificially alter the tension parameter β, holding all other parameters the same. Physically, altering β corresponds to changing the value of Plank's constant. Note that if Plank's constant is zero then the quantum of circulation is zero and $\beta = 0$, which reduces the superfluid to a classical ideal Euler fluid. We find that the column-like motion becomes stronger if β is increased (figure 8*a*) and weaker if β is decreased (figure 8*b*). We conclude that it is the stiffness of the vortex lines which makes the superfluid rotate about the inner cylinder in this way. The macroscopic field u^s_ϕ is the average effect of a great number of microscopic eddies around each vortex line, and these lines do not like to bend too much.

A natural question which arises from our results is what are the relative effects of vortex tension and mutual friction. We have seen that the vortex tension has a strong effect on the superfluid, causing it to rotate as a column of liquid. On the other

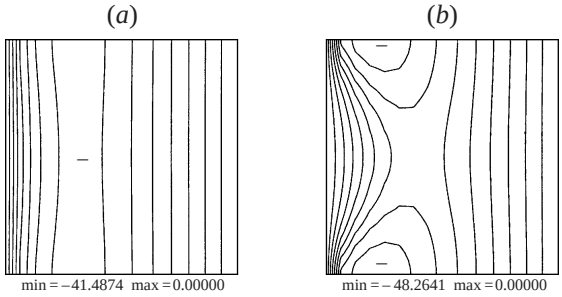

FIGURE 8. Effects on u_ϕ^s of artificially altering the vortex tension parameter β away from its correct value β_{exact}. All runs at $\eta = 0.976$ and $Re = 100$. (*a*) $\beta = 4\beta_{\text{exact}}$; (*b*) $\beta = 0.2\beta_{\text{exact}}$. Compare with the reference state (figure 4*b*).

hand it is the mutual friction which forces the normal fluid to rotate in an opposite direction to the classical case for some values of the parameters.

We can justify the non-classical meridional motion of the superfluid using the following argument: We consider the azimuthal components of the steady-state version of (3.7) evaluated on the ends of the cylinders, $z = 0$ and $z = h$. Applying the relevant boundary conditions we find that

$$0 = \frac{\partial^2 v_\phi^n}{\partial z^2} + \frac{\rho^s}{\rho} F_\phi, \tag{6.1}$$

$$v_r^s \omega_z^s = -\beta T_\phi - \frac{\rho^n}{\rho} F_\phi \tag{6.2}$$

on $z = 0$ and $z = 1$, where ω_z^s represents the total axial superfluid vorticity. We want to show that $v_r^s > 0$ on the end plates indicating that the superfluid will always rotate in the opposite direction to a classical fluid. The azimuthal component of normal fluid velocity, v_ϕ^n, is zero on the ends of the cylinder but will increase rapidly to close to the Couette value in the midplane where the braking effect of the cylinder ends is least. Thus a boundary layer structure will exist at the ends of the cylinders giving $\partial^2 v_\phi^n / \partial z^2 < 0$, and so from (6.1) we find that F_ϕ is positive on the ends of the cylinders. Let us now consider (6.2). Because we are rotating the inner cylinder only, the vortex lines point downwards, thus $\omega_z^s < 0$, and since we have found that $F_\phi > 0$, the mutual friction is forcing the superfluid to rotate counter-classically. Turning our attention to the vortex tension term, we find that on the ends of the cylinders

$$T_\phi = -\text{sgn}\,(\omega_z^s) \frac{\partial \omega_\phi^s}{\partial z}. \tag{6.3}$$

From our numerical results we find that $\partial \omega_\phi^s / \partial z < 0$, in other words the vortex tension is always negative and exerts a classical influence on the Ekman cells; however the sum of the two terms on the right-hand side of (6.2) always results in a negative total. In order to justify this let us assume that the superfluid rotates in the same direction as a classical fluid, in other words, that there is outflow in the centre of the cavity and inflow close to the ends of the cylinders. If this was the case in the lower half of the cavity, the azimuthal component of superfluid vorticity ω_ϕ^s would be positive which together with (4.10) would imply $\partial \omega_\phi^s / \partial z > 0$ resulting in $v_r^s > 0$ from (6.2). This contradicts the assumption that the superfluid rotates in the same direction as

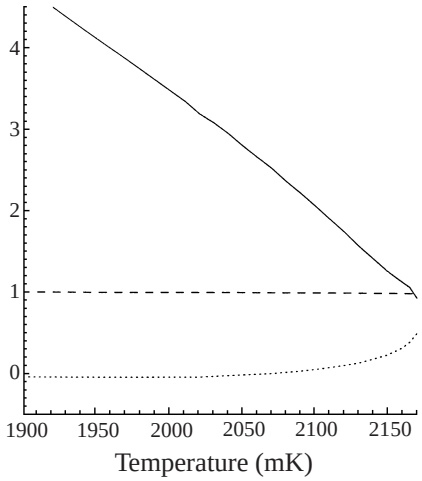

FIGURE 9. The parameters α_1 (dotted line) and α_2 (solid line) as functions of temperature. The dashed line takes the constant value of 1.

a classical fluid. Thus the superfluid must flow in the opposite sense to the classical case, in which case $\partial\omega_\phi^s/\partial z$ will be negative but $v_r^s > 0$.

In conclusion, the meridional motion of $\boldsymbol{v}^s$ is always opposite to that of a classical fluid due to the mutual friction, no matter what the intensity of the mutual friction. We shall now turn our attention to explaining why the normal fluid rotates in a classical direction at temperatures close to $T_\lambda = 2.172\,\mathrm{K}$ but in the opposite direction at lower temperatures. Since $v_r^n = 0$ on the ends of the cylinders we shall obtain an expression for $\partial v_r^n/\partial z$ on $z = 0$ and show that this expression is negative at higher temperatures, indicating classical flow, and positive at lower temperatures, indicating counter-classical flow.

Taking the curl of (2.2) we obtain the following non-dimensional equation for the total superfluid vorticity:

$$\frac{\partial\boldsymbol{\omega}^s}{\partial t} + (\boldsymbol{v}^s\cdot\nabla)\boldsymbol{\omega}^s - (\boldsymbol{\omega}^s\cdot\nabla)\boldsymbol{v}^s = -\beta(\nabla\times\boldsymbol{T}) - \frac{\rho^n}{\rho}(\nabla\times\boldsymbol{F}). \tag{6.4}$$

Evaluating the azimuthal component of (6.4) on $z = 0$ and $z = 1$ we find

$$\frac{\partial v_r^n}{\partial z} = -\frac{\beta}{|\omega_z^s|}\frac{\partial^2\omega_{\phi^s}}{\partial z^2} + \alpha_1\frac{\omega_z^s}{|\omega_z^s|}\frac{\partial v_\phi^n}{\partial z} - \alpha_2\frac{\beta}{\omega_z^s}\frac{\partial^2\omega_r^s}{\partial z^2} \tag{6.5}$$

where the temperature-dependent parameters are given by

$$\alpha_1 = -\frac{B'}{B} \quad \text{and} \quad \alpha_2 = \left(\frac{2\rho - \rho^n B'}{\rho^n B}\right).$$

Considering the terms on the right-hand side of (6.5), we find from our numerical results that both $\partial^2\omega_r^s/\partial z^2$ and $\partial^2\omega_\phi^s/\partial z^2$ are positive on $z = 0$ and since v_ϕ^n will increase away from $z = 0$ the term $\partial v_\phi^n/\partial z$ will be positive there. Thus the first term on the right-hand side of (6.5) will always be negative and the contribution to $\partial v_r^n/\partial z$ from the last two terms will depend on the magnitude and sign of parameters α_1 and α_2. These parameters are plotted in figure 9. The dotted and solid lines represent α_1 and α_2 respectively, with the dashed line taking the constant value of 1. It can be seen that α_1 is positive for $2.06 < T < 2.172$ and decreases rapidly as the temperature

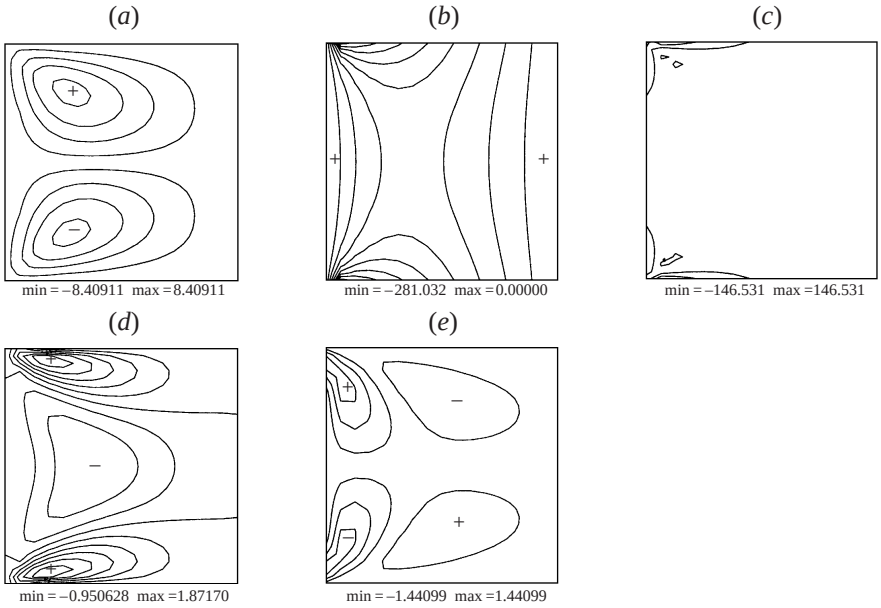

FIGURE 10. Results for the normal fluid at higher Reynolds number $Re = 300$ at $T = 2.11\,\mathrm{K}$ and $\eta = 0.976$. The corresponding results for the superfluid are shown in figure 11. (*a*) Stream function ψ^n; (*b*) azimuthal velocity u^n_ϕ; (*c*) azimuthal vorticity ω^n_ϕ; (*d*) radial velocity u^n_r; (*e*) axial velocity u^n_z.

decreases. For temperatures below 2.05 K α_1 is small and negative. Thus the second term on the right-hand side of (6.5) is negative for $2.06 < T < 2.172$ and decreases in magnitude as the temperature is reduced below $T_\lambda = 2.172\,\mathrm{K}$. It can be seen that α_2 is always positive and increases linearly with decreasing temperature from a value close to unity at $T = 2.17\,\mathrm{K}$. Thus the third term on the right-hand side of (6.5) is positive and increases in magnitude as the temperature decreases. Thus we have explained our findings for the normal fluid. At higher temperatures the negative terms on the right-hand side of (6.5) dominate resulting in the normal fluid moving in a classical way; however as the temperature is reduced, the positive terms increase and the negative terms decrease in magnitude resulting in $\partial v^n_r/\partial z > 0$ and thus the normal fluid Ekman cells rotate in the opposite sense to a classical fluid.

We have also explored the flow pattern at increasing Reynolds numbers up to $Re = 300$; see the plots for the normal fluid and the superfluid in figures 10 and 11 respectively. Apart from the expected stronger layers near the boundaries, the only effect is that u^s_ϕ is more z-dependent.

Even though the mutual friction parameters B and B' are well known, we have performed a series of numerical experiments by artificially changing their values in order to determine the relative roles of the two terms in the mutual friction force (2.6). Changing B' or setting it equal to zero does not make a qualitative difference. However decreasing B means that relatively the vortex tension force becomes more important and we observe that v^s_ϕ becomes more columnar as discussed earlier.

Finally we have considered the flow at different values of aspect ratio. Starting from the reference state at $\eta = 0.976$, we have decreased η. We have found that if $\eta \leqslant 0.85$ the normal fluid Ekman cells rotate in the 'classical' direction, that is in the opposite direction to the superfluid.

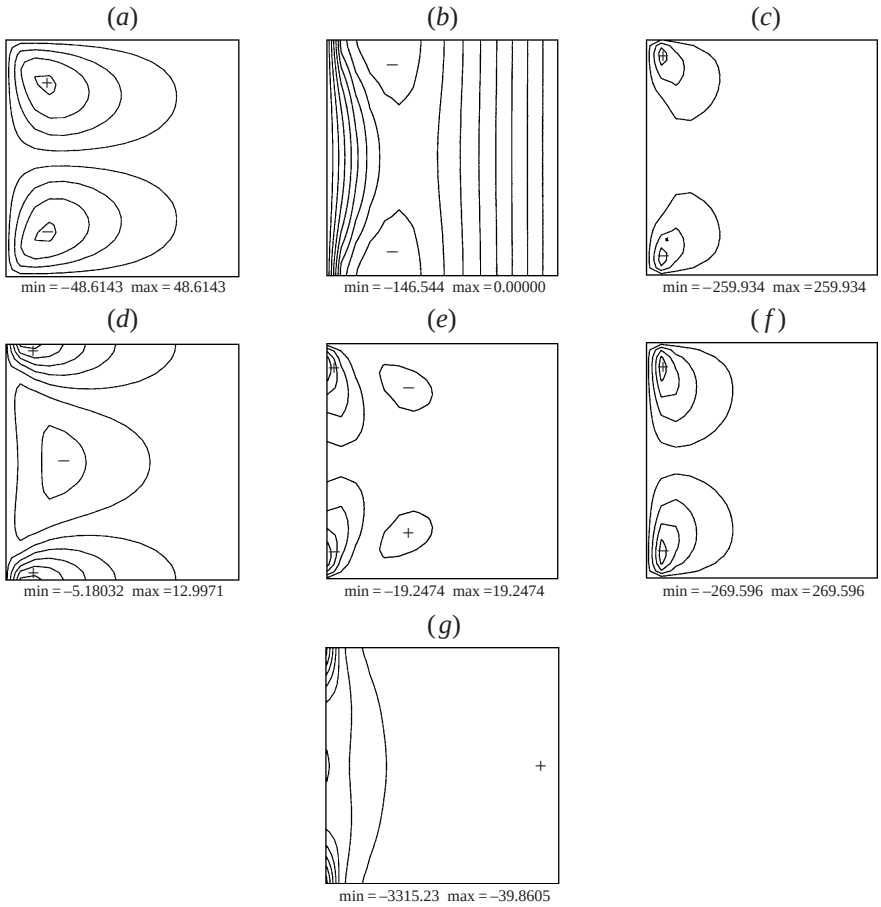

FIGURE 11. Results for the superfluid at higher Reynolds number $Re = 300$ at $T = 2.11\,\mathrm{K}$ and $\eta = 0.976$. The corresponding results for the normal fluid are shown in figure 10. (*a*) Stream function ψ^s; (*b*) azimuthal velocity u^s_ϕ; (*c*) azimuthal vorticity ω^s_ϕ; (*d*) radial velocity u^s_r; (*e*) axial velocity u^s_z; (*f*) radial vorticity ω^s_r; (*g*) axial vorticity ω^s_z.

7. Conclusions

We have considered a very simple flow in a closed rotating cavity to study how the superfluid vortex lines respond to a shear in the presence of boundaries both parallel and perpendicular to the rotation axis, which is the natural direction of alignment of the vortices. The problem has also allowed us to study the boundary conditions of the HVBK equations. A major aim has been to gain more insight into the flow of helium II, which, because of the low temperature environment, cannot be observed directly like a classical fluid.

The main result of our investigation is the anomalous motion of helium II when compared to the motion of a classical fluid. It is also remarkable that even in the simple laminar flow problem which we have considered the normal fluid and the superfluid components of helium II can move in ways which are very different to each other. The first interesting finding is caused by the stiffness of the vortex lines which resist bending; the vortex tension forces the superfluid to rotate around the inner cylinder almost like a rigid column, slipping at the top and bottom plates. The lower the temperature the more pronounced this effect is, because the superfluid

component has more mass and thus determines the dynamics of the entire helium II. Since the vortex lines' stiffness is determined by Plank's constant, this is an effect which highlights the nature of helium II as a quantum fluid rather than a mere inviscid Euler fluid. The second interesting result is that the superfluid Ekman cells always rotate in the opposite direction to that of a classical Navier–Stokes fluid, for which the inflow is near the end plates. This non-classical meridional motion is due to the mutual friction. The third interesting result is that the normal fluid Ekman cells need not be the same as the motion of a classical Navier–Stokes fluid. In most cases we have found that the normal fluid moves in the opposite direction, due to the mutual friction forcing.

All these results give more insight into the hydrodynamics of helium II and how it differs from the motion of a classical fluid. Because of the low temperature environment, it is very difficult to visualize helium II directly, unlike the pattern of a classical fluid such as water or oil which is immediately visible to the experimentalist. More insight into the motion of helium II is clearly needed to understand the current experimental work on helium II turbulence and its relation with classical turbulence.

The natural development of our work is to study how end effects influence the transition from Couette flow to Taylor vortices as the temperature is reduced.

C.F.B.'s research on the subject is funded by an equipment grant of the Royal Society of London. K.L.H. gratefully acknowledges the support of the Nuffield Foundation.

REFERENCES

Aarts, R. G. K. M. & deWaele, A. T. A. M. 1994 Numerical investigation of the flow properties of He II. *Phys. Rev.* B **50**, 10069–10079.

Barenghi, C. F. 1992 Vortices and the Couette flow of helium II. *Phys. Rev.* B **45**, 2290–2293.

Barenghi, C. F., Bauer, G., Samuels, D. S. & Donnelly, R. J. 1997 Superfluid vortex lines in a model of turbulent flow. *Phys. Fluids* **9**, 2631–2643.

Barenghi, C. F., Donnelly, R. J & Vinen, W. F. 1983 Friction on quantised vortices in helium II. *J. Low Temp. Phys.* **52**, 189–247.

Barenghi, C. F. & Jones, C. A. 1987 The stability of superfluid helium between rotating concentric cylinders. *Phys. Lett.* A **122**, 425–430.

Barenghi, C. F., Swanson, C. J. & Donnelly, R. J. 1995 Emerging issues in helium turbulence. *J. Low Temp. Phys.* **100**, 385–413.

Bendt, P. J. 1967 Attenuation of second sound in helium II between rotating cylinders. *Phys. Rev.* **153**, 280–284.

Bielert, F. & Stamm, G. 1993 Visualisation of Taylor Couette flow in superfluid helium. *Cryogenics* **33**, 938–940.

Bielert, F. & Stamm, G. 1994 Influence of quantized vortex lines on the stability of Taylor Couette flow in He II. *Physica* B **194**, 561–562.

Chandrasekhar, S. 1961 *Hydrodynamics and Hydromagnetic Stability*. Oxford University Press.

Chandrasekhar, S. & Donnelly, R. J. 1957 The hydrodynamics stability of helium II between rotating cylinders. *Proc. R. Soc. Lond.* A **241**, 9–28.

Cliffe, K. A. 1983 Numerical calculation of two-cell and single-cell Taylor flows. *J. Fluid Mech.* **135**, 219–233.

Donnelly, R. J. 1991*a* *High Reynolds Number Flows Using Liquid and Gaseous Helium*. Springer.

Donnelly, R. J. 1991*b* *Quantized Vortices in Helium II*. Cambridge University Press.

Donnelly, R. J. & Lamar, M. M. 1988 Flow and stability of helium II between rotating cylinders. *J. Fluid Mech.* **186**, 163–198.

Donnelly, R. J. & Swanson C. E. 1986 Quantum turbulence. *J. Fluid Mech.* **173**, 387–429.

Feynman, R. P. 1955 Application of quantum mechanics to liquid helium. In *Progress in Low Temperature Physics*, vol. 1 (ed. C. J. Gorter). North Holland.

Fiszdon, W., Piechna, J., Stamm, G. & Olszok, T. 1994 Boundary layer influence on He II flows. *Physica* B **194**, 587–588.

Geurst, J. A. 1979 Mutual friction in the laminar flow of superfluid helium II through capillary tunes. *Phys. Lett*. A **71**, 78–82.

Hall, H. E. 1960 The rotation of helium II. *Phil. Mag. Suppl.* **9**, 89–146.

Hall, H. E. & Vinen, W. F. 1956 The rotation of helium II. (part 2): the theory of mutual friction in uniformly rotating helium II. *Proc. R. Soc. Lond*. A **238**, 215–234.

Henderson, K. L. & Barenghi, C. F. 1994 Calculation of torque in nonlinear Taylor vortex flow of helium II. *Phys. Lett*. A **191**, 438–442.

Henderson, K. L., Barenghi, C. F. & Jones, C. A. 1995 Nonlinear Taylor Couette flow of helium II. *J. Fluid Mech.* **283**, 329–340.

Hills, R. N. & Roberts, P. H. 1977 Superfluid mechanics for a high density of vortex lines. *Arch. Rat. Mech. Anal*. **66**, 43–71.

Khalatnikov, I. M. 1965 *An Introduction to the Theory of Superfluidity*. Benjamin.

Landau, L. D. & Lifshitz, E. M. 1987 *Fluid Mechanics*. Pergamon.

Lucke, M., Mihelicic, K. & Wingerath, K. 1984 Flow in a small annulus between concentric cylinders. *J. Fluid Mech.* **140**, 343–353.

Maurer, J. & Tabeling, P. 1998 Local investigations of superfluid turbulence. *Europhys. Lett*. **43**, 29–34.

Melotte, D. J. & Barenghi, C. F. 1998 Transition to normal fluid turbulence in helium II. *Phys. Rev. Lett*. **80**, 4181–4184.

Nemirowskii, S. K. & Fiszdon, W. 1995 Chaotic quantized vortices and hydrodynamic process in superfluid helium. *Rev. Mod. Phys*. **67**, 37–84.

Nore, C., Abid, M. & Brachet, M. E. 1997*a* Decaying Kolmogorov turbulence in a model of a superflow. *Phys. Fluids* **9**, 2644–2669.

Nore, C., Abid, M. & Brachet, M. E. 1997*b* Decaying Kolmogorov turbulence in low-temperature superflows. *Phys. Rev. Lett*. **78**, 3896–3899.

Pfister, G., Schmidt, H., Cliffe, K. A. & Mullin, T. 1988 Bifurcation phenomena in Taylor–Couette flow in a very short annulus. *J. Fluid Mech.* **191**, 1–18.

Samuels, D. C. 1992 Velocity matching and Poiseuille pipe flow of helium. *Phys. Rev*. B **46**, 11714–11724.

Samuels, D. C. & Donnelly, R. J. 1990 Dynamics of the interaction of rotons with quantized vortices in helium II. *Phys. Rev. Lett*. **65**, 187–190.

Schwarz, K. W. 1982 Generating superfluid turbulence from simple dynamical rules. *Phys. Rev. Lett*. **49**, 283–285.

Schwarz, K. W. 1985 Three dimensional vortex dynamics in superfluid ^{4}He. Line-line and line-boundary interaction. *Phys. Rev*. B **31**, 5782–5804.

Schwarz, K. W. 1988 Three dimensional vortex dynamics in superfluid ^{4}He. *Phys. Rev*. B **38**, 2398–2417.

Smith, M. R., Donnelly, R. J., Goldenfeld, N. & Vinen, W. F. 1993 Decay of vorticity in homogeneous turbulence. *Phys. Rev. Lett*. **71**, 2583–2586.

Snyder, H. A. 1974 Rotating Couette flow of superfluid helium. *Proc. 13th Intl Conf. Low Temp. Phys., LT13*, vol. 1, pp. 283–287. Plenum.

Sonin, E. B. 1987 Vortex oscillations and hydrodynamics of rotating superfluids. *Rev. Mod. Phys.* **59**, 87–155.

Swanson, C. E. & Donnelly, R. J. 1987 The appearance of vortices in the flow of helium II between rotating cylinders. *J. Low Temp. Phys*. **67**, 185–193.

Swanson, C. E., Wagner, W. T., Donnelly, R. J. & Barenghi, C. F. 1987 Calculation of frequency dependent and velocity dependent mutual friction parameters in Helium II. *J. Low Temp. Phys*. **66**, 263–276.

Swanson, C. J. & Donnelly, R. J. 1991 The instability of Taylor Couette flow of helium II. *Phys. Rev. Lett*. **67**, 1578–1581.

Thouless, D. J., Ao, P. & Niu, Q. A. 1996 Transverse force on a quantized vortex in a superfluid. *Phys. Rev. Lett*. **76**, 3758–3761.

Tough, J. T. 1982 Superfluid turbulence. In *Progress in Low Temperature Physics*, vol. 8 (ed. D. F. Brewer). North Holland.